Electronic Supplementary Material (ESI) for Nanoscale.

Supplementary Information to "Forming-free and self-rectifying resistive switching of the simple Pt/TaO_x/n-Si structure for access device-free high-density memory application"

Shuang Gao, Fei Zeng,[a)]* Fan Li, Minjuan Wang, Haijun Mao, Guangyue Wang, Cheng Song and Feng Pan[b)]*

Laboratory of Advanced Materials (MOE), School of Materials Science and Engineering, Tsinghua University, Beijing 100084, People's Republic of China

[a)]E-mail: zengfei@mail.tsinghua.edu.cn. Tel.: +86-10-62795373

[b)]E-mail: panf@mail.tsinghua.edu.cn. Tel.: +86-10-62772907

SI1. The detailed parameters adopted during the fitting process of XPS spectra

All XPS spectra were fitted by the use of XPS Peak4.1. The energy separation and area ratio between the $4f_{5/2}$ and $4f_{7/2}$ peaks in a Ta 4*f* doublet were fixed to be 1.8 eV and 3:4, respectively. The FWHM parameters for the $4f_{5/2}$ and $4f_{7/2}$ peaks in a Ta 4*f* doublet were taken to be equal. The % Lorentzian-Gaussian parameters for all Ta 4*f*, Si 2*p*, and O 1*s* peaks were constrained to the same search range between 10% and 30%.

SI2. The analysis of O 1*s* XPS spectra

Fig. SI2 shows the XPS spectra of O 1*s* from a TaO_x/n-Si bi-layer structure after etching by Ar^+ ion beam (1 keV) of 40 (upper) and 200 s (lower). All spectra can be well fitted by a main peak (blue) at ~531.3 eV and a mall peak (red) at ~532.2 eV. The blue peak at ~531.3 eV corresponds definitely to the Ta–O binding.[1] The red peak is ~1 eV higher than the blue one and is attributed to the Si–O binding and/or to the contamination.[2] Since there is no signal of Si 2*p* after an etching of 40 s (Fig. 1b in the main text), the upper red peak with a small area percentage of 16% should originate from the contamination. After an etching of 200 s, the area percentage of the red peak increases significantly to 32%. Given the appearance of Si 2*p* signal after 200 s etching (Fig. 1b in the main text), this significant increase in area percentage is reasonably contributed by the Si–O binding, thus supporting the existence of an interfacial SiO_y layer.

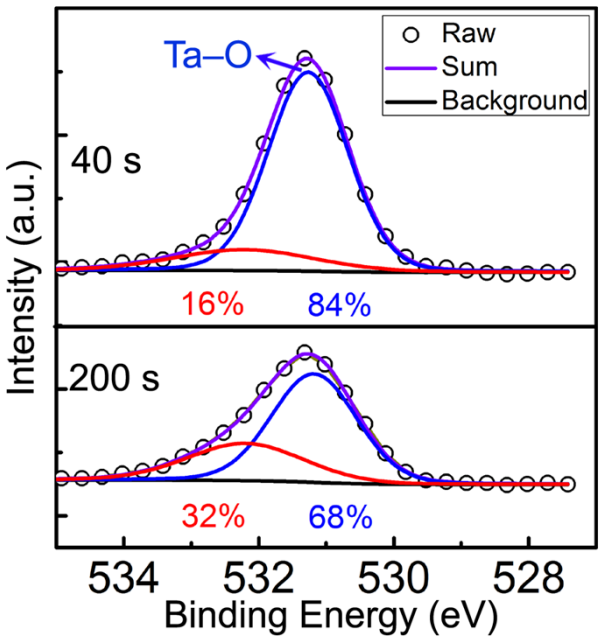

Fig. SI2 XPS spectra of O 1*s* obtained from a TaO_x/n-Si bi-layer structure after etching by Ar^+ ion beam (1 keV) of 40 (upper) and 200 s (lower). The area percentage of each peak is shown in the inset.

SI3. The detailed calculation process for read margin

To calculate the read margin, analytical expressions for the *I*–*V* curves of both LRS and HRS under both positive and negative voltage polarities should be obtained first. Fig. SI3a shows the comparison between experimental data and fitting curves based on the following analytical expressions:

$$\log(I_{\mathrm{LRS},+}) = -9.9691 + 8.13367 \cdot V + 10.66664 \cdot V^2 - 21.90367 \cdot V^3 + 9.27006 \cdot V^4$$

$$|I_{\mathrm{LRS},-}| = 1.8 \times 10^{-11} \times \exp(10 \cdot |V|^{0.5})$$

$$I_{\mathrm{HRS},+} = 8 \times 10^{-10} \times [\exp(3 \cdot V) - 1]$$

$$|I_{\mathrm{HRS},-}| = 8 \times 10^{-10} \times [\exp(2.1 \cdot |V|) - 1]$$

The little difference between experimental data and fitting curves supports the rationality of these analytical expressions.

Fig. SI3b shows the equivalent circuit of an $N \times N$ ($N \geq 2$) crossbar array using OBPU approach and under the worst case scenario for reading a LRS cell. For a given combination of (V_{pu}, R_{pu}, N), the following four equations with four variables (i.e., V_1, V_2, V_3, and $V_{\mathrm{out,LRS}}$) can be obtained on the basis of Kirchhoff's circuit laws:

$$V_1 + V_2 + V_3 - V_{\mathrm{out,LRS}} = 0$$

$$(N-1) \times I_{\mathrm{HRS},+}(V_1) - (N-1)^2 \times |I_{\mathrm{HRS},-}|(V_2) = 0$$

$$(N-1) \times I_{\mathrm{HRS},+}(V_1) - (N-1) \times I_{\mathrm{HRS},+}(V_3) = 0$$

$$V_{\mathrm{out,LRS}} + R_{\mathrm{pu}} \times [I_{\mathrm{LRS},+}(V_{\mathrm{out,LRS}}) + (N-1) \times I_{\mathrm{HRS},+}(V_1)] - V_{\mathrm{pu}} = 0$$

Based on these four equations and the analytical expressions, $V_{\mathrm{out,LRS}}$ for the given combination of (V_{pu}, R_{pu}, N) can be numerically calculated by using MATLAB. Similarly, $V_{\mathrm{out,HRS}}$ for the given combination of (V_{pu}, R_{pu}, N) can be obtained. Then read margin for

the given combination of (V_{pu}, R_{pu}, N) can be calculated according to ($V_{out,HRS} - V_{out,LRS}$)/$V_{pu}$ × 100%. With this calculation method for read margin, a series of ($V_{out,LRS}$, $V_{out,HRS}$, read margin) combinations corresponding to a given (V_{pu}, R_{pu}) combination can be calculated by varying the value of N. The Fig. 3c in the main text is plotted based on the calculated ($V_{out,LRS}$, $V_{out,HRS}$, read margin) combinations corresponding to the (1.1 V, 6 000 Ω) combination with the vary of N from 2 to 300 with an increment of 1. One can easily see from Fig. 3c that, on the premise of 10% read margin, N_{max} is 212 for the (1.1 V, 6 000 Ω) combination. The Table 1 in the main text is drawn based on the obtained N_{max} values corresponding to a series of (V_{pu}, R_{pu}) combinations (V_{pu} varies from 0.8 to 1.2 V with an increment of 0.1 V and R_{pu} varies from 2 000 to 12 000 Ω with an increment of 2 000 Ω).

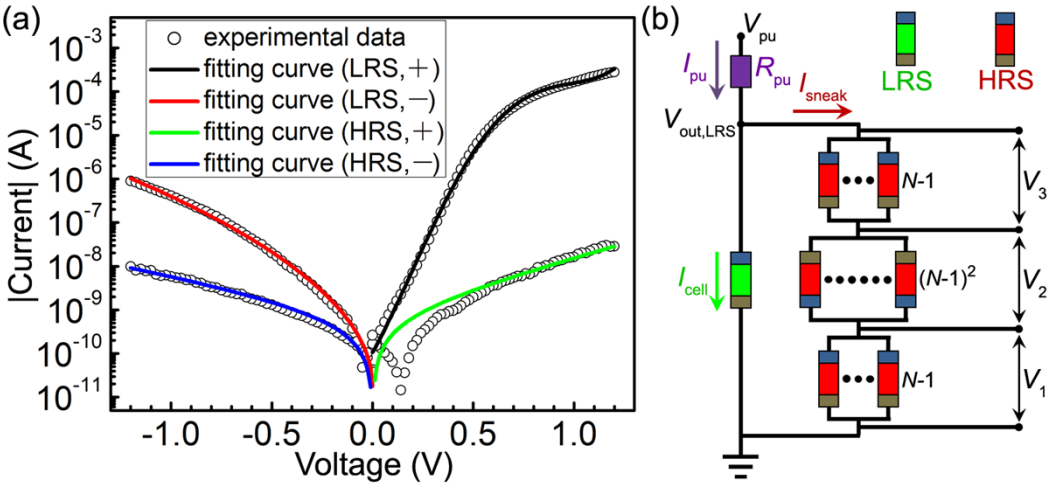

Fig. SI3 (a) A comparison between experimental data and fitting curves based on analytical expressions. (b) Equivalent circuit of an N×N ($N \geq 2$) crossbar array using OBPU approach and under the worst case scenario for reading a LRS cell.

SI4. The explanation for the image-force lowering effect

Based on Ref. S3, the relation between current density J and interfacial electric field E for thermionic emission is as follows:

$$J = A^{**} \cdot T^2 \cdot \exp\left(\frac{-q \cdot \left(\Phi_B - \sqrt{(q \cdot E)/(4 \cdot \pi \cdot \varepsilon_r \cdot \varepsilon_0)} \right)}{k_B \cdot T} \right) \quad (1)$$

where A^{**} is the effective Richardson constant, T is the absolute temperature, q is the electron charge, Φ_B is the Schottky barrier height without image-force lowering effect, k_B is the Boltzmann constant, ε_r is the high-frequency relative permittivity of the insulator, and ε_0 is the vacuum permittivity. In equation (1), the term subtracting from Φ_B is due to the image-force lowering effect. Considering $I = J \cdot A^*$ (A^* is the device area) and $E = V/t$ (t is the thickness of the insulator), equation (1) can be rewritten as

$$I = A^* \cdot A^{**} \cdot T^2 \cdot \exp\left(\frac{-q \cdot \left(\Phi_B - \sqrt{(q \cdot V)/(4 \cdot \pi \cdot \varepsilon_r \cdot \varepsilon_0 \cdot t)} \right)}{k_B \cdot T} \right) \quad (2)$$

Equation (2) can be simplified to

$$\ln(I) = A \cdot V^{0.5} + B \quad (3)$$

where

$$A = \frac{q}{k_B \cdot T} \sqrt{q/(4 \cdot \pi \cdot \varepsilon_r \cdot \varepsilon_0 \cdot t)} \quad (4)$$

and

$$B = \ln\left(A^* \cdot A^{**} \cdot T^2 \right) - \frac{q \cdot \Phi_B}{k_B \cdot T} \quad (5)$$

Hence, it can be easily seen that the image-force lowering effect is revealed by the term of $A \cdot V^{0.5}$. The value of A can be obtained by fitting the measured I–V characteristic of the

HRS under negative voltage polarity. Subsequently, ε_r can be calculated on the basis of equation (4).

SI5. The analysis of Schottky barrier height and activation energy for hopping conduction at various voltages

The analysis of Schottky barrier height and activation energy for hopping conduction has been done in a voltage region from 0.05 to 0.5 V with an interval of 0.05 V. The obtained results are displayed in Fig. SI5. Fig. SI5a shows the plot of $\ln(I/T^2)$ *vs*. $1/(k_B \cdot T)$ at various voltages for the LRS and corresponding fitting curves. The absolute fitting slope values are denoted by the navy squares in Fig. SI5b. The red circles in this figure represent the Schottky barrier height values that are calculated based on the method in Ref. S4. It can be seen that the Schottky barrier height spreads between ~0.30 to ~0.43 eV with an average value of ~0.37 eV. Fig. SI5c shows the plot of $\ln(I)$ *vs*. $1/(k_B \cdot T)$ at various voltages for the LRS and corresponding fitting curves. The absolute fitting slope values, i.e., the activation energy values for hopping conduction, are denoted by the navy squares in Fig. SI5d. It can be seen that the activation energy decreases linearly with the voltage, which is in line with the result in Ref. S5 and further supports the correctness of hopping conduction for the HRS.

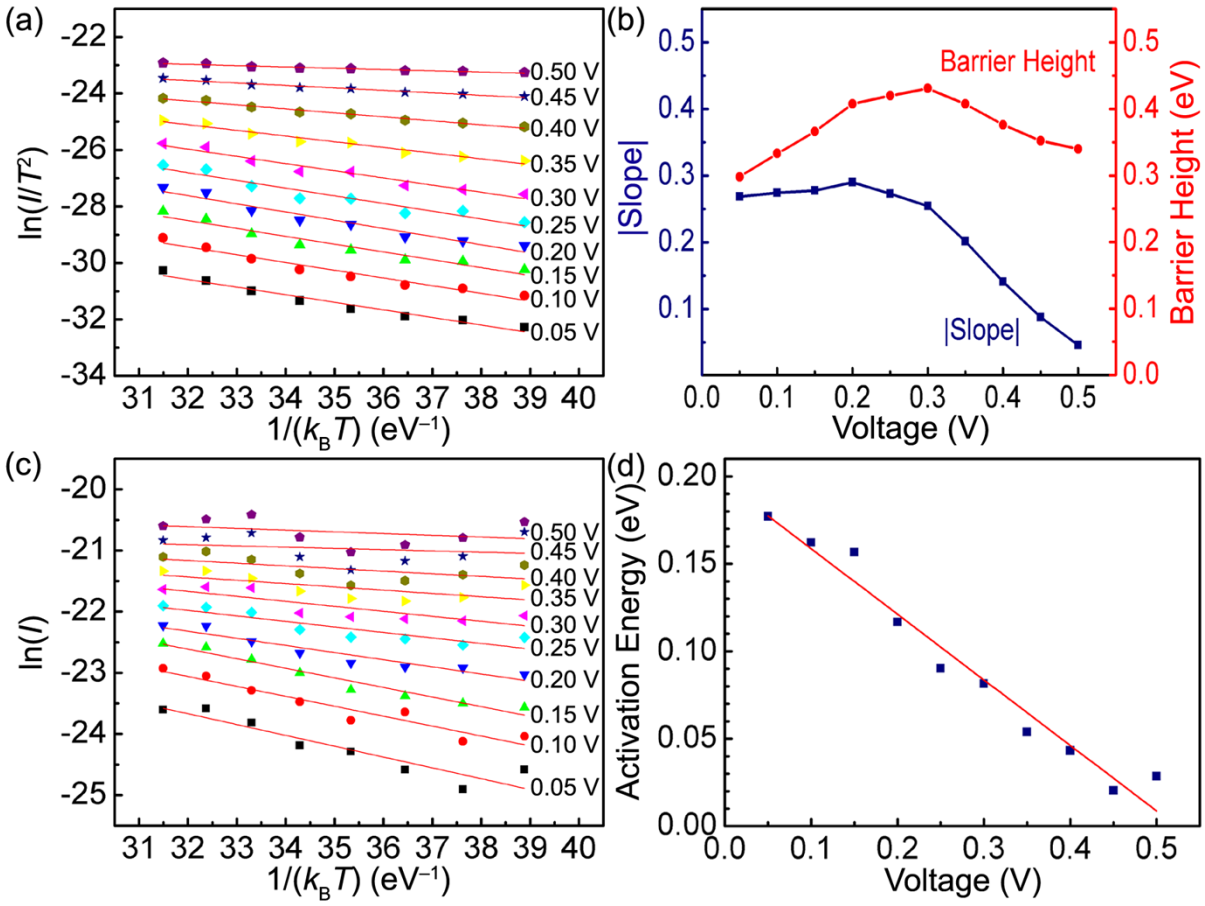

Fig. SI5 (a) The plot of $\ln(I/T^2)$ *vs*. $1/(k_B \cdot T)$ at various voltages for the LRS and corresponding fitting curves. (b) The voltage-dependent fitting slope and barrier height for the LRS. (c) The plot of $\ln(I)$ *vs*. $1/(k_B \cdot T)$ at various voltages for the HRS and corresponding fitting curves. (d) The voltage-dependent activation energy for the HRS and corresponding fitting curve.

SI6. The discussion on the low activation energy of 0.12 eV for hopping conduction

Based on Refs. S6–S8, we can obtain three activation energy values for hopping conduction in various TaO_x-based MIM tri-layer structures. Also, the current density under an external electric field of 0.2 MV/cm for each tri-layer structure can be roughly extracted. Fig. SI6 shows the relation between the activation energy and the current density. It is apparent that the activation energy decreases significantly with the current density. Since a larger current density under a fixed external electric filed is certainly caused by a higher V_O concentration in the TaO_x layer, it can be deduced that the activation energy for hopping conduction decreases with the V_O concentration in the TaO_x layer. This is because an increase in the V_O concentration means a decrease in the distance between two adjacent V_Os and consequently an increase in the overlap between electron wavefunctions of them.[9] For our Pt/TaO_x/n-Si RRAM devices in the HRS, a current value of 9.975×10^{-11} A is measured with an external voltage of 0.2 V, as shown in the inset of Fig. SI6. Considering the device diameter of 300 μm and the TaO_x thickness of ~10 nm, a current density of $\sim 1.4 \times 10^{-7}$ A/cm^2 is obtained at an external electric field of ~0.2 MV/cm. The activation energy has been calculated to be 0.12 eV in the main text. Hence, we can add the data point for our Pt/TaO_x/n-Si tri-layer structure in Fig. SI6. It can be seen that the data point in this work accords well with the tendency of previous experimental data. This supports the correctness of our experimental result and our explanation that the low activation energy of 0.12 eV for hopping conduction can be reasonably attributed to the abundant V_Os in our TaO_x layer.

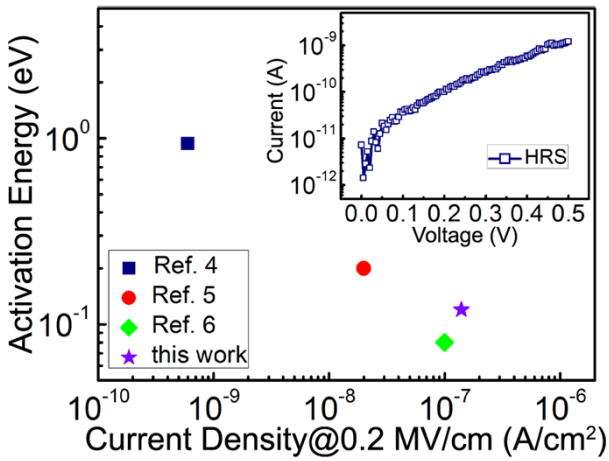

Fig. SI6 The relation between the activation energy for hopping conduction and the current density under an external electric field of 0.2 MV/cm for TaO_x-based MIM tri-layer structures. The inset shows the *I–V* characteristic of the Pt/TaO_x/n-Si RRAM devices in the HRS.

SI7. The discussion on resistance-dependent V_{set}, V_{reset}, and I_{reset}

Fig. SI7a shows the R_{HRS}-dependent V_{set}. The V_{set} is defined by the same method as that in the main text, while the R_{HRS} is defined by referring to Ref. S10. The data points in this figure are extracted based on the same original data as that for the cycle-to-cycle switching uniformity in the main text except 20 switching cycles with a gradual set process. From a statistical point of view, $|V_{set}|$ decreases with the R_{HRS}, which is just opposite to the result in Ref. S10. This is most likely caused by the series resistance of the Pt/TaO_x interface. During the set process, the Schottky-like Pt/TaO_x barrier is reversely biased and consequently acts as a series resistor with a large resistance. Therefore, to set the device with a lower R_{HRS}, a higher $|V_{set}|$ is needed to compensate the more obvious voltage drop at the Pt/TaO_x interface.

The R_{LRS}-dependent V_{reset} and I_{reset} are shown in Figs. SI7b and SI7c, respectively. The R_{LRS} is defined by the same method as that in the main text, while the V_{reset} and I_{reset} are defined by referring to Ref. S11. The data points in these two figures are also extracted based on the same original data as that for the cycle-to-cycle switching uniformity in the main text. From a statistical point of view, the V_{reset} increases slightly with the R_{LRS}, while the I_{reset} decreases with the R_{LRS} approximately in accordance with $I_{reset} \propto 1/R_{LRS}$. These results suggest that the power consumption of reset process can be reduced by increasing the R_{LRS}, i.e., on the expense of reducing ON/OFF ratio.

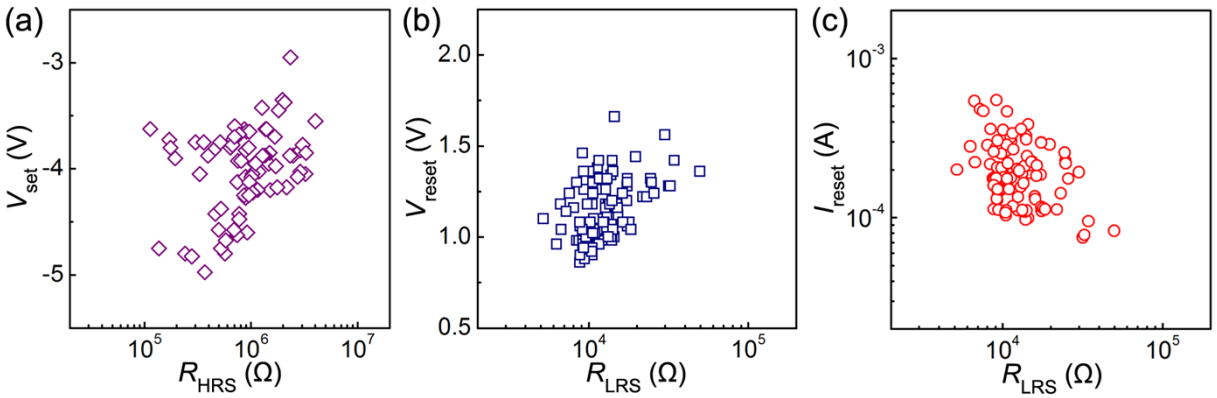

Fig. SI7 (a) The R_{HRS}-dependent V_{set}. The R_{LRS}-dependent (b) V_{reset} and (c) I_{reset}.

SI8. References

S1. E. Atanassova, G. Tyuliev, A. Paskaleva, D. Spassov and K. Kostov, *Appl. Surf. Sci.*, 2004, **225**, 86–99.

S2. L. Kornblum, B. Meyler, J. Salzman and M. Eizenberg, *J. Appl. Phys.*, 2013, **113**, 074102.

S3. Physics of Semiconductor Devices, ed. S. M. Sze and K. K. Ng, John Wiley & Sons, Inc., Hoboken, New Jersey, 3rd edn., 2006.

S4. W. J. Liu, X. A. Tran, H. Y. Yu and X. W. Sun, *ECS Solid State Lett.*, 2013, **2**, Q35−Q38.

S5. Y. Yang, S. Choi and W. Lu, *Nano Lett.*, 2013, **13**, 2908−2915.

S6. A. Persano, F. Quaranta, M. C. Martucci, P. Cretì, P. Siciliano and A. Cola, *J. Appl. Phys.*, 2010, **107**, 114502.

S7. S. Banerjee, B. Shen, I. Chen, J. Bohlman, G. Brown and R. Doering, *J. Appl. Phys.*, 1989, **65**, 1140.

S8. S. Ezhilvalavan and T.-Y. Tseng, *Thin Solid Films*, 2000, **360**, 268–273.

S9. S. Choi, Y. Yang and W. Lu, *Nanoscale*, 2014, **6**, 400–404.

S10. S. Long, X. Lian, T. Ye, C. Cagli, L. Perniola, E. Miranda, M. Liu and J. Suñé, *IEEE Electron Device Lett.* 2013, **34**, 999–1001.

S11. S. Long, X. Lian, T. Ye, C. Cagli, L. Perniola, E. Miranda, M. Liu and J. Suñé, *IEEE Electron Device Lett.* 2013, **34**, 623–625.